JOURNAL OF MATERIALS SCIENCE **34** (1999) 291–299

The mechanical behavior of foamed aluminum

H. FUSHENG, Z. ZHENGANG
Laboratory of Internal Friction and Defects in Solids, Institute of Solid State Physics, Chinese Academy of Sciences, Hefei 230031, People's Republic of China
E-mail: fshan@mail.issp.ac.cn

Experiments have been carried out to investigate the mechanical behavior of foamed aluminum with different matrixes and states. It is found that the matrix composition has a significant influence over the deformation, failure and fracture of foamed aluminum. Like other cellular solid materials, Al foam shows a smooth compression stress–strain curve with three regions characteristic of plastic foams: linear elastic, plastic collapse and densification. AlMg10 foam has a serrated plateau and no densification, characteristic of brittle foams. AlMg10 foam has higher compressive and tensile strength but lower ductility than Al foam. The difference in the mechanical properties between Al foam and AlMg10 foam decreases as the relative density decreases, and when it is lower than roughly 0.15, no difference can be discerned. The mechanical properties in compression are clearly higher than those in tension, which can be explained in terms of dislocation theory and stress concentration behavior.

1. Introduction

Porous metals have long been commercially important materials of practical use in a wide variety of applications [1]. Recently, those with macropores have attracted extensive attention for their excellent functional properties. One example is foamed aluminum (FA) [2]. It has a higher porosity ranging from 60% to 85% and low bulk density. While its functional properties such as acoustic absorption [3], mechanical damping [4], energy absorption [5, 6] and electromagnetic shielding [7] have been comprehensively studied and well understood, few studies on its structural properties have been reported, and its mechanical response to applied stress is still unclear. For a functional material, the durability or lifetime of the function is an important property and should be taken into consideration; it is directly related to the material's mechanical properties. Therefore, the mechanical properties of FA such as strength, deformation and damage were investigated to provide valuable information for applications.

2. Experimental procedure

2.1. Preparation of FA specimens

FA blocks were manufactured by a melting foaming process using commercially pure aluminum and aluminum–10% magnesium alloy. The whole process consists of five steps:

(i) Melting the metal ingot at 700 °C;
(ii) Adding MnO_2 powder (mean particle size of 20 μm) into the melt and stirring it at a speed of 800 r.p.m. to make it become a viscous fluid;
(iii) Introducing TiH_2 powder (mean particle size of 40 μm) into the modified melt and stirring it at an increased speed of 2300 r.p.m. to distribute the powder uniformly in the melt;
(iv) Holding the mixture at 625 °C for 120 s, allowing the TiH_2 to decompose and release hydrogen gas, allowing the bubbles to evolve;
(v) Removing the melt together with the crucible from the furnace and cooling them by air blowing.

Cylindrical specimens, with a diameter of 30 mm and a length of 40 mm, were then cut by electrosparking from the cast blocks. The density of each specimen was calculated from a measurement of its mass and volume. The calculation of relative density is based on the density of 2.7 g cm^{-3} for commercially pure aluminum and 2.55 g cm^{-3} for AlMg10 alloy, respectively. Some AlMg10 foam specimens were subjected to solution treatment at a temperature of 454 ± 5 °C for 20 h.

2.2. Apparatus

A uniaxial compression and a uniaxial tension test were performed with an Autograph universal testing machine (Shimadzu Corp., Tokyo, Japan, AG-A Series, Computer Control System). The strain rate was 2×10^{-2} mms^{-1}. Stress is defined as the load per total area of the specimen, including porosity. Likewise, the strain is defined as a nominal value for the foam structure and is not the true strain experienced in the cell walls. The structure morphology of the foam was examined using conventional light microscopy and scanning electron microscopy.

3. Results

3.1. Structure morphology of FA

Fig. 1 exhibits two typical structures of FA. A pore size gradient and a density gradient exist in the structure

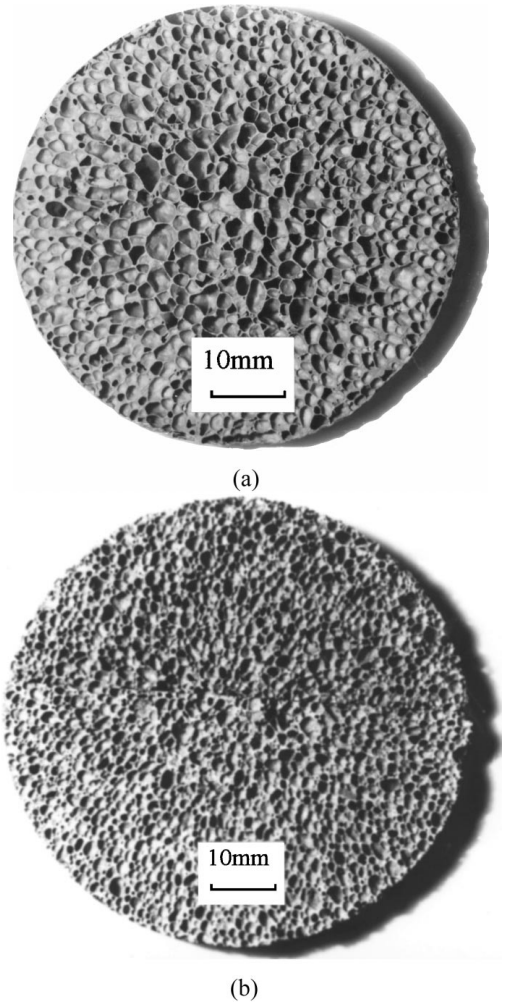

Figure 1 Typical structures of FA: (a) Al foam and (b) AlMg10 foam.

of commercially pure aluminum foam (Al foam). The foam has larger pores and a lower density in the middle and significantly smaller pores and a higher density near the boundary. In contrast, aluminum–10% magnesium alloy foam (AlMg10 foam) has quite a uniform pore and density distribution through the section. The pores in both foams are irregular ellipsoids and most are closed.

3.2. The stress–strain behavior in compression

Typical compression curves for several Al and AlMg10 foams are shown in Fig. 2a–c. Al foam has a smooth stress–strain curve, characteristic of plastic foams [8], with three distinct regions: a linear elastic region; a long plateau where the stress is almost independent of strain; and a final region of densification in which the stress–strain curve rises steeply. In contrast, AlMg10 foam shows a rather different curve. As-cast AlMg10 foam has a serrated plateau region, a pronounced feature of brittle foam [9]. After solution-treatment, the magnitude of the load oscillations during serrated fracture is substantially reduced compared to that of as-cast samples, which implies some improvement of ductility. Both AlMg10 foams show no densification regions.

The stress–strain curves show linear elastic behavior at small strains (approximately less than 0.05) which seems to be independent of the matrix and its state. The difference in the plateau between Al foam and AlMg10 foam is clearly ascribed to different deformation mechanisms, which will be discussed in the following sections.

Densification starts for Al foam when the cell walls touch. The strain boundary defining the start of densification is given by [10]

$$\varepsilon_s = 1 - 2\frac{\rho}{\rho_s} \tag{1}$$

where ρ/ρ_s is the initial relative density of Al foam. Obviously the strain at which densification starts decreases as the relative density increases, which is demonstrated by Fig. 2a.

3.3. Compressive deformation feature

As seen in Fig. 3, after the initiation of collapse there are both deformed and undeformed regions in the structures of both Al and AlMg10 foam, i.e. complete collapse of some parts has occurred while the rest is still elastic. Therefore, two strain states coexist at almost the same stress. The collapse bands increase in size with increasing strain until the whole specimen collapses. In Al foam, pore collapse occurs essentially by plastic yielding of the cell walls throughout the entire deformation bands and the yielding appears in a layer roughly perpendicular to the direction of compressive stress. In contrast, AlMg10 foam collapses by brittle fracture of the cell walls, and no yielding modes are discerned. At a higher strain, longer cracks penetrate through the uncollapsed region, and the interface between the collapsed region and the uncollapsed region is no longer a plane. The rupture induces the cell walls to break into many small pieces, and the stress is therefore relaxed. As the compression proceeds, the broken structure is squeezed together and the stress again rises until the next fracture occurs, which is responsible for the serrations in the plateau.

Fig. 4a and b shows two locally magnified collapse structures of Al foam and AlMg10 foam, respectively. In the structure of Al foam, the plastic bending and the overlapping of the cell walls are quite significant, while rupture is indiscernible. But in the structure of AlMg10 foam, serious brittle fracture takes place and isolated fragments (as indicated by A) can be clearly seen near the fractured surface. The fractured surface shows a jagged pattern, and some of the surface has been squeezed together (as shown by B). These features further demonstrate the difference in the collapse modes of Al foam and AlMg10 foam.

3.4. The compressive strength

For fair comparison of different foams, we define the stress at 0.02 offset strain as the yield strength ($\sigma_{0.02}$) of FA in view of the stress–strain curves. As shown in Figs 2 and 5, AlMg10 foam has a much higher $\sigma_{0.02}$

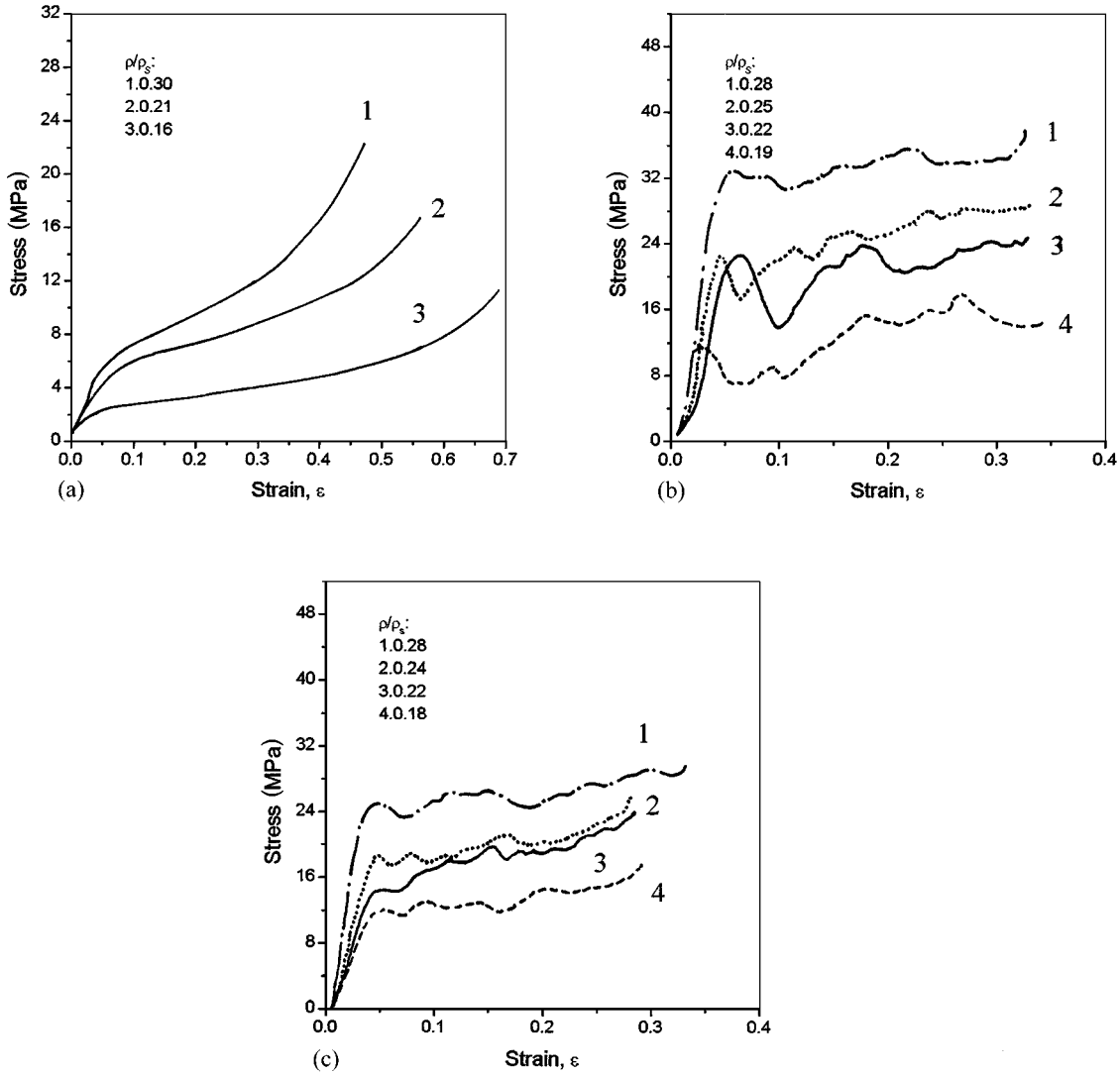

Figure 2 Compressive stress–strain curves of FA: (a) Al foam and (b) AlMg10 foam (as-cast); (c) AlMg10 foam (solution treated).

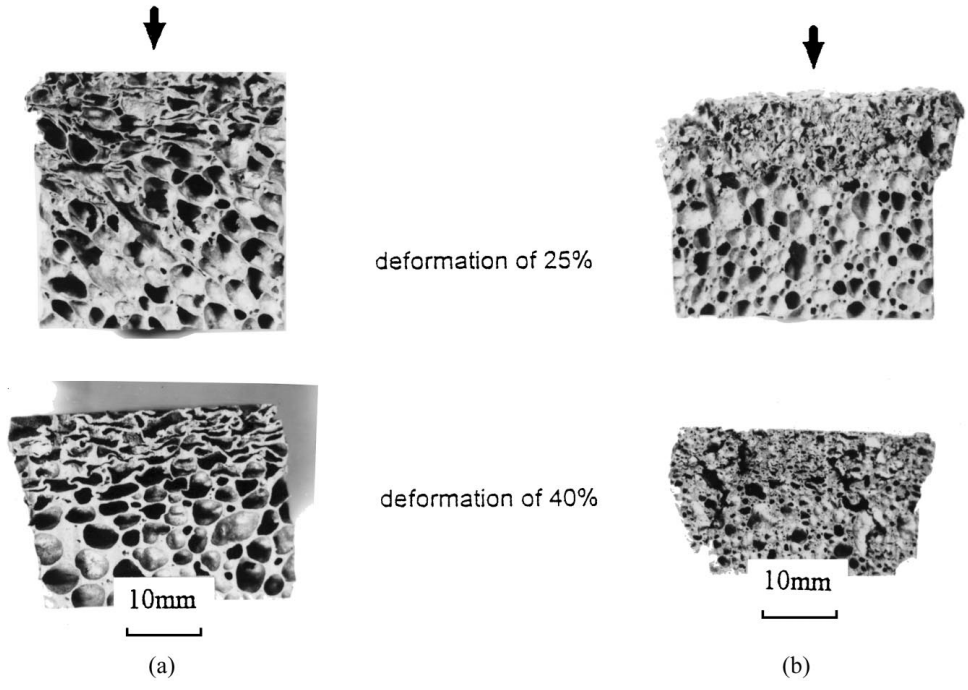

Figure 3 Deformation development of FA: (a) Al foam and (b) AlMg10 foam.

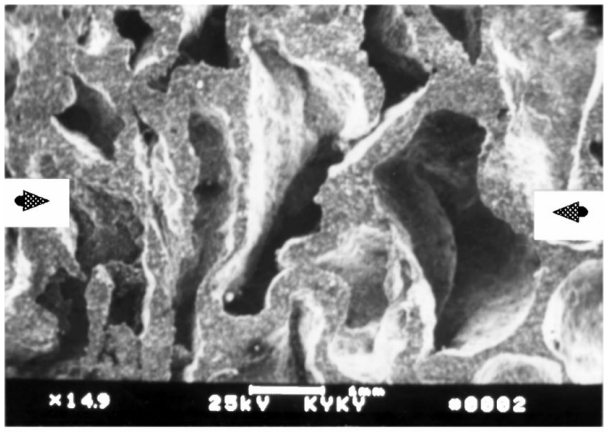

(a)

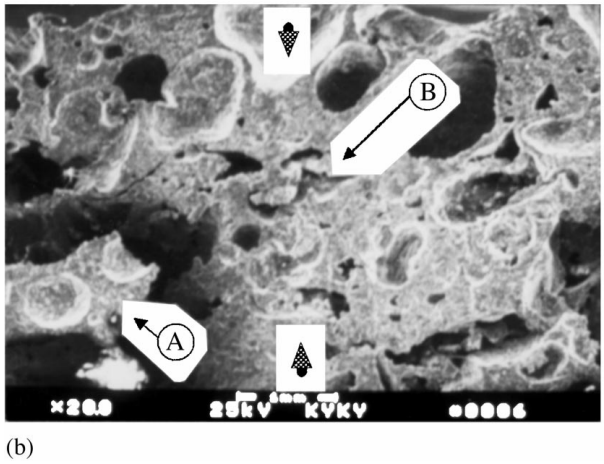

(b)

Figure 4 The morphology of collapse structures of FA: (a) Al foam and (b) AlMg10 foam.

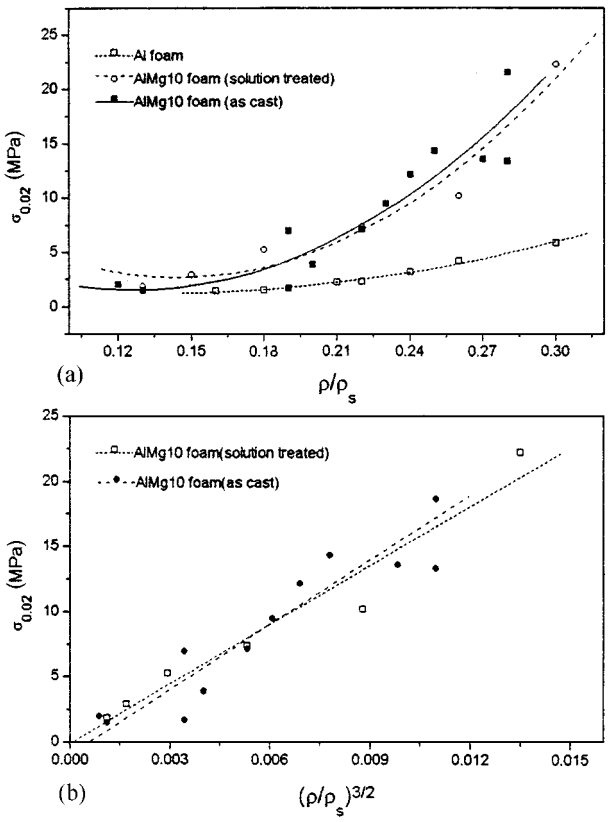

Figure 5 (a) Yield strength versus relative density and (b) yield strength versus the power of 3/2 of relative density.

than Al foam, consistent with their corresponding matrix since block Al–10% Mg alloy also has much higher strength than commercially pure Al. The increase of the yield or crushing strength of FA with the relative density is consistent with the expected behavior of FA, but the dependence is obviously non-linear. The solution treatment shows little influence on the compressive strength of AlMg10 foam.

3.5. The stress–strain behavior in tension

Typical tensile stress–strain curves are shown in Fig. 6 for different relative densities and foams. For Al foam, the curves show linear elastic behavior at a strain of roughly 0.02, much smaller than that in compression, followed by plastic yielding and strain hardening up to the peak stress. For AlMg10 foam, the stress–strain curves show a very sharp peak at strains less than 0.04 and little or no yield could be found. The peak becomes a little wider after solution treatment, suggesting that the plastic deformation increases before fracture. As in compression, the offset strain increases with increasing relative density, but is much smaller than that in compression. In addition, as the relative density decreases, the Young's modulus, the yield strength and the slope of the stress–strain curve through the plastic collapse region all decrease.

3.6. Tensile fracture feature

Micrographs of a typical fracture surface are shown in Fig. 8. The cell walls can be seen to form ridges and the outline is clear and smooth, corresponding to its smooth stress–strain curves. In contrast, the fracture surface of AlMg10 foam exhibits a rather rough morphology, a typically brittle fracture feature. Solution treatment seems to have little influence on this morphology. It can be argued that the Al foam failed due to the stable propagation of cracks, while the propagation of cracks in AlMg10 foam is multidirectional and much quicker.

3.7. The ductility in tension

Fig. 7 shows the influences of relative density, matrix composition and state on the ductility (δ_{gt}) of FA. Of the three foams, Al foam has a maximum δ_{gt}, whereas AlMg10 foams of different states show roughly the same value. However, the difference in ductility between Al foam and AlMg10 foam rapidly decreases with decreasing relative density, and when it reaches a value around 0.15, no difference can be found. From the above results, we know that AlMg10 foam is a brittle foam, while Al foam is a plastic one. Therefore, the value of 0.15 seems to be a critical value of relative density, below which even plastic foams may become completely brittle.

According to the dislocation theory of plastic deformation, the ductility of a crystalline material depends on the mobility of dislocations in the structure. The former is determined either by the dislocation–dislocation interaction, direct dislocation–particulates interaction

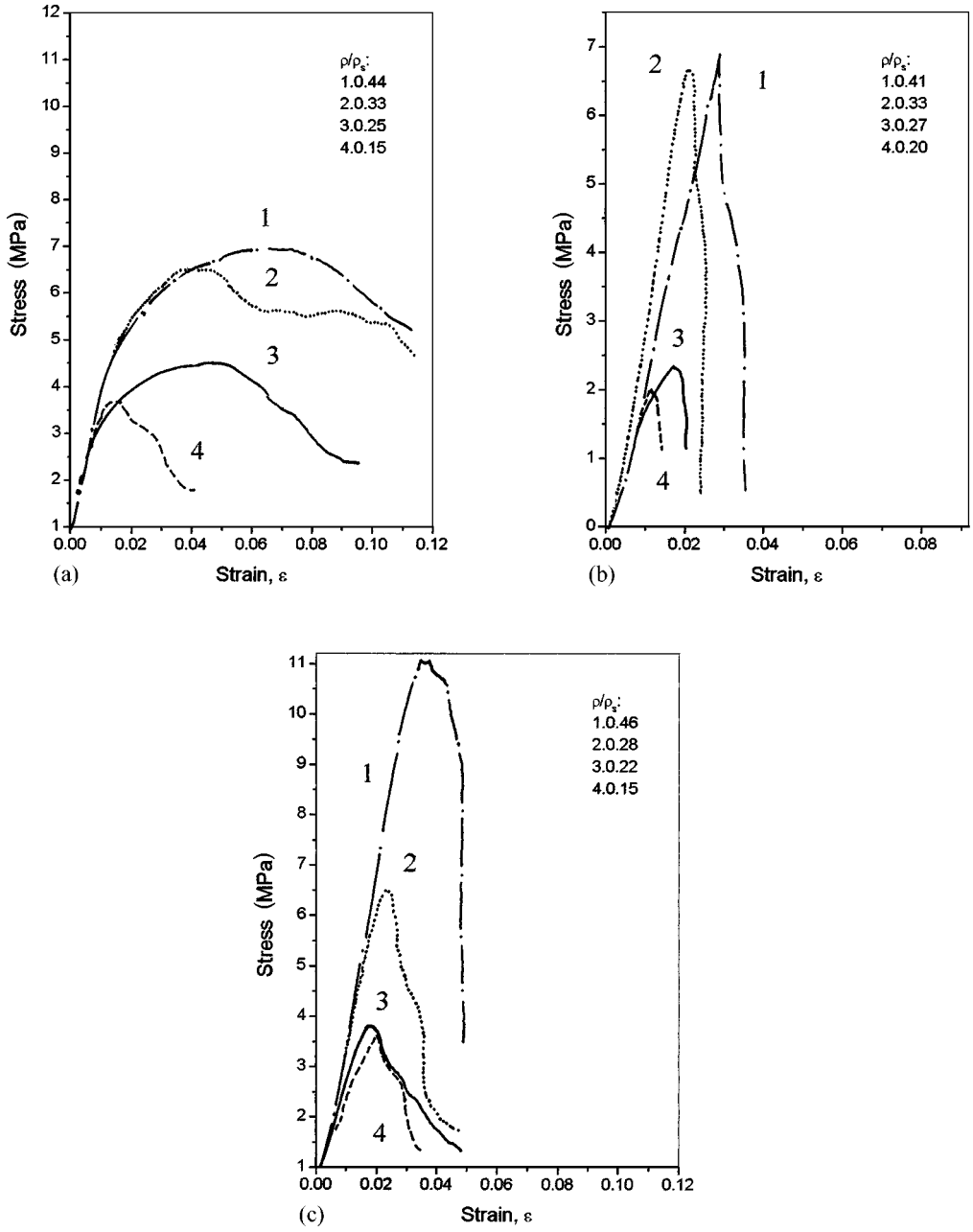

Figure 6 Tensile stress–strain curves of FA: (a) Al foam; (b) AlMg10 foam (as-cast) and (c) AlMg10 foam (solution treated).

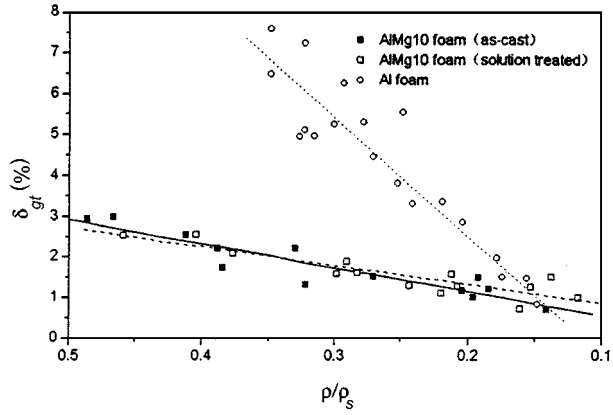

Figure 7 Variation of δ_g versus relative density.

or by indirect dislocation-particulates interaction [11]. In general, high dislocation density and dispersed particulates may resist the movement of dislocations. Previous results showed that there were substantial dislocations and other defects in the microstructure of FA, particularly around the pores [4]. Dislocation mobility is therefore strongly constrained, leading to a lower ductility. Thus both Al foam and AlMg10 foam show much lower ductility in tension than that in compression. Furthermore, in the microstructure of as-cast AlMg10 foam there are quantities of brittle β phase (Mg_2Al_3) particulates distributed along the α grain boundaries [12], where high dislocation density is generated as a result of differential thermal contraction caused by the difference in the coefficient of thermal expansion of the two phases. Under tensile loading, dislocations will pile up surrounding the β particulates due to their pinning effect, initiating high degree of stress concentration [13]:

$$\tau = n\tau_0 \tag{2}$$

where τ is the stress imposed on the pinning points, n is the number of dislocations and τ_0 is the applied stress.

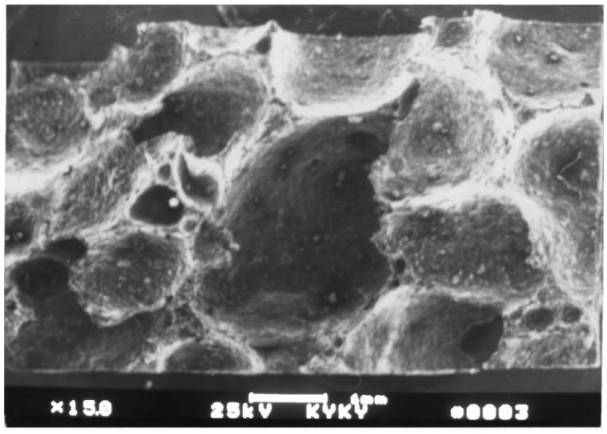

(a)

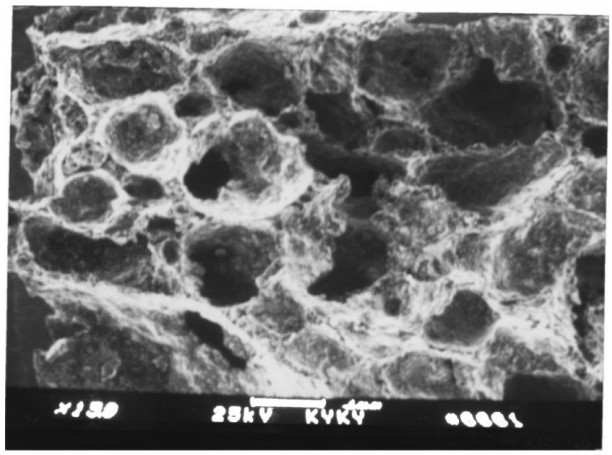

(b)

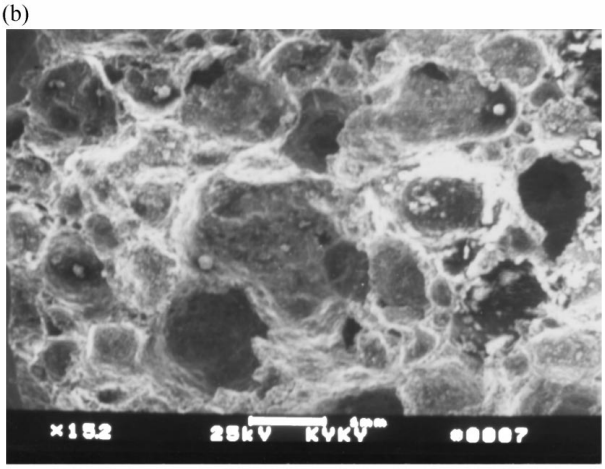

(c)

Figure 8 Morphologies of fracture surface. (a) Al foam and (b) AlMg10 foam (as-cast); (c) AlMg10 foam (solution treated).

Since the β phase is very brittle, cracks can readily propagate across it and combine with each other in many directions after the initiation of cracks in the grain boundaries, leading to brittle crushing. Therefore, AlMg10 foam exhibits a much lower ductility than Al foam. From the sudden drop of the stress–strain curves, it is recognized that the propagation of cracks is very rapid and the failure of the specimen is catastrophic.

3.8. Tensile strength

The yield strength and ultimate tensile strength are plotted against relative density in Fig. 9. The dependence of the strengths on relative density follows a significantly

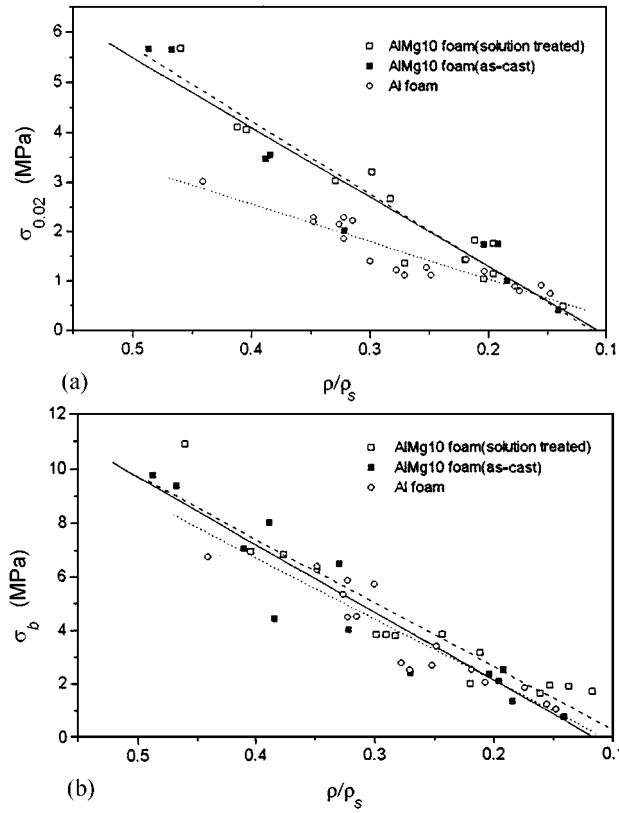

Figure 9 Tensile strength versus relative density: (a) yield strength and (b) ultimate strength.

linear relationship. This trend is quite different from that in compression, in which the yield strength and relative density follow a fractional power relationship (Fig. 5).

Some researchers regard porous materials as a particular two-phase solid composed of voids and cell walls, whose strengths obey a simple law of mixtures [14]. Results for porous Cu by Simone and Gibson [15] were consistent with this theory. However, the present study shows that FA does not obey this law. From Fig. 9, the yield and ultimate tensile strength, for instance, of the solid cell wall material, estimated from the intercept of the linear regression, are about 12.5 MPa and 19.5 MPa respectively, which are much smaller than the handbook values of both metals. This implies that the weakening effect of pores on the strengths is not solely determined by the number of pores.

During the fabrication of FA, numerous bubbles originate in the melt. During the subsequent cooling, they will hinder the solidification contraction of the melt, forming a high degree of thermal stress and even micro-cracks in the cell walls. Thus, in addition to pores, stress concentration and micro-cracks certainly impose an additional weakening effect accentuating the failure under a relative smaller tensile loading, leading to a much smaller strength than that deduced from the law of mixtures.

As shown in Fig. 9, the metal matrix has a pronounced effect on the tensile yield strength and is similar to the situation in compression; AlMg10 foam also has a higher yield strength than Al foam. Nevertheless, the matrix has only a slight influence over the ultimate strength.

It can also be noted that, like the δ_{gt}, the discrepancy between the tensile yield strength for different foams decreases as the relative density decreases and the critical value of the relative density is also approximately 0.15. This trend suggests that as the relative density decreases, the contribution of the matrix composition to the overall mechanical properties decreases, and when the relative density is below 0.15, the contribution is too small to be detected. Thus it appears that selection of a stronger matrix for FA may be of importance only for a relative density greater than 0.15.

The effect of solution treatment is rather indiscernible, similar to the effect of compression. This is perhaps because the strengthening due to the solution treatment is balanced by the weakening induced by the pores.

4. Discussion

4.1. The compressive deformation models of cellular solid materials

There have been several models describing the compressive deformation and mechanical properties of cellular materials, the more recent of which is presented by Ashby and Gibson *et al.* [10]. They predicted that the compressive stress–strain curve of cellular solids, whether elastomeric, plastic or brittle, can be divided into three regions: the linear elastic, the plateau and the densification regions. The extent of each region depends on its relative density and responds to different mechanical behavior.

Ashby and Gibson, in terms of the cubic model of an open-cell cellular material and Euler's equation, derived a series of equations to describe the mechanical properties of a cellular solid. Those relating to the present investigation are listed below.

(i) Linear elastic region:
$$\frac{E^*}{E_s} = \left(\frac{\rho}{\rho_s}\right)^2 \tag{3}$$

(ii) Plateau region: for plastic foam
$$\frac{\sigma^*_{pl}}{\sigma_Y} = C_1\left(\frac{\rho}{\rho_s}\right)^{\frac{3}{2}} \tag{4}$$

for brittle foam
$$\frac{\sigma^*_f}{\sigma_f} = C_2\left(\frac{\rho}{\rho_s}\right)^{\frac{3}{2}} \tag{5}$$

Stress–strain response:
$$\frac{\sigma}{\sigma_Y} = C_3\left(\frac{\rho}{\rho_s}\right)^{\frac{3}{2}} \times \left\{\frac{1-\left(\frac{\rho}{\rho_s}\right)^{\frac{1}{3}}}{1-\left[\frac{\rho}{\rho_s}\left(\frac{1}{1-\varepsilon}\right)\right]^{\frac{1}{3}}}\right\} \tag{6}$$

where E^* is the Young's modulus of foam, E_s is the Young's modulus of the cell wall material, σ^*_{pl} is the plastic collapse stress of plastic foam, σ_Y is the yield strength of cell wall material, σ^*_f is the crushing strength of brittle foam, σ_f is the modulus of rupture of cell wall material, σ is the compressive stress, and C_1 and C_2 are constants.

As seen in Fig. 1, FA has a dominantly closed cell structure. Nevertheless, a number of experiments have proven that most foams behave as if their cells were open, because surface tension concentrates material into the cell edges during their manufacture [10, 16]. The faces are frequently so thin that they contribute very little to the overall stiffness and strength, particularly when the relative density is very low, and the mechanical properties of a closed cell material can be treated as that of an open one. Since the relative density of the present specimens is in the range of 0.1–0.3, this corresponds to the condition of a "thin" face. Furthermore, the cell collapse initiates from plastic bending (for Al foam) or brittle fracture (for AlMg10 foam) of the cell walls, similar to the failure of a beam, as shown in Figs 3 and 4. Thus the mechanical behavior of FA in compression can be well described by the Gibson–Ashby model. The linear dependence of the compressive strength on the 3/2 power of relative density shown in Fig. 5 provides a good example.

4.2. Comparing tensile strength with compressive strength

A constitutive model for porous materials indicated that the porosity acted as a hardening mechanism when the material was subjected to overall hydrostatic compression and as a softening mechanism for overall hydrostatic tension [17]. Thus the tensile strength is lower than the compressive strength for most porous materials. The present study shows the same trend, though some different results have been obtained by other investigators [8].

Both theory and experiment have proven that voids or cracks are more harmful to the mechanical properties of materials in tension than in compression. Consider a crack of length c in an elastic solid, lying normal to a remote tensile stress σ (Fig. 10), that creates a singular stress field [8]

$$\sigma_l = \sigma\sqrt{\frac{c}{2r}} \tag{7}$$

at a distance r from its tip. Because $c \gg r$ and $\sigma_l \gg \sigma$, the resulting stress concentration at the tip will fracture the cell walls locally, thus extending the flaw and leading to sudden fracture and thus produce a lower tensile strength. Evidently this stress concentration does not exist in compression.

As mentioned above, high thermal stress can be generated during the fabrication of FA and hot cracks are inevitably initiated in the high thermal stress region, because of the relatively low thermal strength in the process of solidification. Thus, these cracks together with "softer" pores are the major origin of low tensile strength.

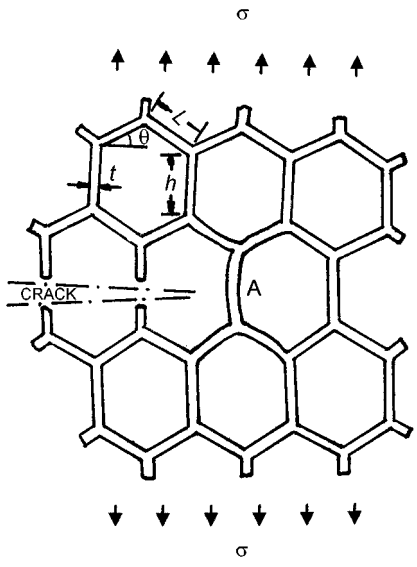

Figure 10 Propagation of a crack through a foam loaded in tension.

The present investigation shows that the tensile properties of FA have obvious linear relationships with the relative density, while the compressive strength is proportional to the fractional power (3/2) of the relative density.

Gibson *et al.* [8] pointed out that the moment on the first unbroken cell wall (marked A) beyond the crack tip is

$$M = \int_0^{(h+l\sin\theta)/2} \sigma_l b \left(\frac{h + l\sin\theta}{2} - r \right) dr \qquad (8)$$

where b is the depth of the honeycomb cell (normal to the page), and r is the distance from the crack tip. From this equation, the tensile strength for loading in the h direction is given by

$$\frac{\sigma^*}{\sigma_s} = \frac{1}{4\sqrt{2}\cos^{3/2}\theta} \sqrt{\frac{l}{c}} \left(\frac{t}{l} \right)^2 \qquad (9)$$

where σ^* and σ_s are the fracture stress of foam and of cell-wall material, respectively, and c is the length of a crack.

From the preceding paragraph, the pores of FA in the present study can be simplified as open ones in view of the Gibson–Ashby dimensional argument model. Thus, we obtain

$$\left(\frac{t}{l} \right)^2 \propto \left(\frac{\rho}{\rho_s} \right) \qquad (10)$$

From Equation 9, it can be shown that

$$\sigma^* \propto \frac{\rho}{\rho_s} \qquad (11)$$

i.e. the tensile strength of FA is proportional to its relative density, consistent with the present results.

5. Conclusions

A study has been carried out to examine the structural morphology and mechanical behavior of foamed aluminum with two different matrixes under compressive and tensile loading.

The pores in present foamed aluminum specimens are irregular ellipsoids and most are closed ones. The foamed aluminum made of commercially pure aluminum shows a smooth compressive stress–strain curve with three distinct regions: linear elastic, plastic collapse plateau and densification region. Its failure originates from the plastic bending of cell walls, characteristic of plastic foams. However, that made of Al-10% Mg alloy shows a serrated plateau and no densification region. It fails by brittle crushing of the cell walls, consistent with brittle foams.

In addition to different responses to applied stress, foams with different matrixes show different mechanical properties. AlMg10 foam has a higher compressive and tensile strength but lower ductility than Al foam. The effects of the matrix on the mechanical properties decrease with decreasing relative density. When the relative density decreases to roughly 0.15, no observable difference can be found between different foams. This suggests that selection of a stronger matrix may be helpful only when the relative density of a foam is relatively large, say greater than 0.15.

The mechanical behavior of foamed aluminum in compression is in agreement with the Gibson–Ashby dimensional argument model. The compressive strength of foamed aluminum follows a fractional power relationship with the relative density, while the tensile strength decreases linearly with decreasing relative density, which can be explained by a beam bending model. Foamed aluminum has lower mechanical properties in tension than in comression, where it suffers from the rapid propagation of cracks under tensile stress. Unlike the composition, the matrix state has only a slight influence on the mechanical behavior of foamed aluminum.

References

1. M. KELLOMAKI, J. ASTROM and J. TIMONEN, *Phys. Rev. Lett.* **77** (1996) 2730.
2. V. SHAPOVALOV, *MRS Bull.*, (1994) 24.
3. H. FUSHENG, Z. ZHENGANG and L. CHANGSONG, *Acustica/Acta Acust*. to be published in June, 1998.
4. H. FUSHENG, Z. ZHENGANG and L. CHANGSONG, *Scr. Metall. Mater*. **37** (1997) 1441.
5. P. H. THORNTON and C. L. MAGEE, *Metall. Trans. A* **6** (1975) 1253.
6. H. FUSHENG, Z. ZHENGANG and L. CHANGSONG, *Acta Phys. Sin. (in Chinese)* **47** (1998) 372.
7. M. FUKUSHIMA, T. FUJI and K. KITAZAWA, *Hitachi Shipbuilding Tech. Rep. (in Japanese)* **49** (1988) 41.
8. L. J. GIBSON, M. F. ASHBY, J. ZHANG and T. C. TRIANTAFILLOU, *Int. J. Mech. Sci*. **31** (1989) 635.
9. S. K. MAITI, L. J. GIBSON and M. F. ASHBY, *Acta Metall. Mater.* **32** (1984) 1963.
10. M. F. ASHBY, *Metall. Trans. A* **14** (1983) 1755.
11. I. A. IBRAHIM, F. A. MOHAMED and E. J. LAVERNIA, *J. Mater. Sci*. **26** (1991) 1137.
12. A. B. ERIC, in "*Metals Reference Book*," (6th Edn., Butterworth & Co. Ltd., 1983) pp. 11–40.

13. F. DUAN and Q. DIRONG, in "*Metallurgical Physics*," Vol. 1, Structure and Defects (in Chinese), (Science Press, Beijing, 1987) p. 301.
14. A. EMELYANOV, E. L. FURMAN, I. P. CONACOVA and V. A. BELOGLAZOV, *Adv. Compos. Mater*. **1** (1993) 1.
15. A. E. SIMONE and L. J. GIBSON, *Acta Metall. Mater*. **44** (1996), 1437.
16. L. J. GIBSON and M. F. ASHBY, *Proc. R. Soc. Lond. A* **43** (1982) 382.
17. P. P. CASTAHEDA and M. ZAIDMAN, *J. Mech. Phys. Solids.* **42** (1994) 1459.

Received 10 March
and accepted 17 July 1998